The Astrophysical Journal, 636:1067–1077, 2006 January 10

THE ASYMMETRIC DUST ENVIRONMENT OF IK TAURI

J. Weiner, K. Tatebe, D. D. S. Hale, and C. H. Townes
Space Sciences Laboratory and Department of Physics, University of California, Berkeley, CA 94720;
johnw@ssl.berkeley.edu, tatebe@ssl.berkeley.edu, david@isi.mtwilson.edu, cht@ssl.berkeley.edu

J. D. Monnier
Department of Astronomy, University of Michigan, 501 East University Avenue, Ann Arbor, MI 48109; monnier@umich.edu

M. Ireland and P. G. Tuthill
School of Physics, Sydney University, NSW, 2006, Australia; mireland@Physics.usyd.edu.au, p.tuthill@Physics.usyd.edu.au

R. Cohen
W. M. Keck Observatory, Waimea, HI

and

R. K. Barry, J. Rajagopal, and W. C. Danchi
NASA Goddard Space Flight Center, Code 667, Greenbelt, MD 20771; rkbarry@iri1.gsfc.nasa.gov,
jayadev_rajagopal@yahoo.com, william.c.danchi@nasa.gov
Received 2004 August 4; accepted 2005 September 13

ABSTRACT

Mid-infrared observations of IK Tau have been made at 11.15 μm with the three-telescope Infrared Spatial Interferometer on Mount Wilson and also using individual segments of the Keck telescope for multiple-aperture interferometry on the Keck telescope at 10.7 μm. Both experiments provided closure phase and show temporal variations and asymmetries in the surrounding dust, with a difference of about 15% in intensity between two sides of the star. Asymmetries have been previously observed in the distribution of SiO masers closely surrounding the star. Comparison with earlier interferometric measurements shows substantial reduction in dust surrounding the star over the last decade. Several asymmetric dust models are investigated and simple images constructed.

Subject headings: stars: AGB and post-AGB — stars: atmospheres — stars: individual (IK Tauri) — techniques: interferometric

1. INTRODUCTION

The circumstellar environment of Mira variable stars is characterized by cool temperatures and relatively high densities, leading to a richer chemistry than is found in hotter stars and to formation of solid-state dust grains. Studies of the spectral energy distribution (SED) of O-rich Miras in general and IK Tau in particular have concluded that the dust is composed primarily of silicate grains that form at temperatures around 1000 K (Suh 2002; Danchi et al. 1994). The component of the SED originating in the dust is sensitive to the spatial distribution, thermal profile, and chemistry of the circumstellar shell.

Present measurements provide information in particular on spatial distribution. Visibilities of IK Tau have previously been measured with the two-telescope Infrared Spatial Interferometer (ISI) at 11 μm (Danchi et al. 1994; Hale et al. 1997), and the dust shells (which make up most of the emitted flux at this wavelength) were modeled. With only one baseline no closure phase can be measured (Baldwin et al. 1986), and hence the two-telescope ISI yielded only one spatial frequency at a given projected orientation on the star. This resulted in models generally assuming spherical symmetry. Still, it was clear that a simple description entailing a single shell of dust forming at some radius and its subsequent outflow was invalid. Rather, multiple shells were found to move radially outward with time (Monnier et al. 1997). The recent addition of a third telescope to the ISI, currently in a linear east-west configuration, has now allowed measurements of asymmetries.

Closure phases have previously been measured on IK Tau in the near-infrared using interferometry (Monnier et al. 2004). The stellar size at a wavelength of 2.16 μm appeared to be 20.2 mas, and no significant asymmetry in the dust distribution was observed. The stellar contribution to the total flux at this wavelength is close to 70%. Thus, in the near-IR the cooler, more extended dust provides a much smaller fraction of the radiation than it does in the mid-infrared, and the dominant source of radiation is found at different radii. Some asymmetries have been observed on other AGB stars (Monnier et al. 2000, 2004; Vinković et al. 2004; Biller et al. 2005; Tuthill et al. 2000a, 2005), and many have been interpreted as the beginning stages of the formation of bipolar planetary nebulae. Magnetic effects have been theorized to be a primary means of the breaking of spherical symmetry in dust shells at the end of the star's life (Soker & Zoabi 2002). An unobserved companion, which influences dust formation, can also be responsible for an asymmetry, and such have been reported in other stars (Tuthill et al. 1999).

2. OBSERVATIONS

Interferometry was performed in the mid-infrared on IK Tau on several different dates using both the ISI and the Keck telescope. Dates and stellar phases for the observations are listed in Table 1.

2.1. *ISI Observations*

The ISI, located on Mount Wilson, California, now uses three movable telescopes. Heterodyne detection with a CO_2 laser local oscillator down-converts stellar signals to radio frequencies from which fringes are formed by a combination of signals from two telescopes and visibilities and closure phases recorded. A range of baselines were sampled with the telescopes in fixed positions

TABLE 1
IK Tauri Observations

Date(s)	Wavelength (μm)	Phase[a]	Flux$_{11\ \mu m}$ (Jy)
2003 Sep 16–18	11.149	0.83	3900
2003 Dec 16–17	11.149	0.02	4600
2004 Sep 1	10.7	0.58	
2004 Sep 15–17	11.149	0.61	3000
2004 Nov 18–19	11.149	0.75	3300

[a] Phase estimate based on visible photometry provided by AAVSO.

separated by 4, 8, and 12 m in an east-west array. Baselines referred to below are designated (1-2), (2-3), and (3-1) for the 4, 8, and 12 m separations between telescopes, respectively. The Earth's rotation provides a range of projected baselines. A description of the older two-telescope ISI can be found in Hale et al. (2000), with additions necessary for the measurement of closure phase described in Hale et al. (2003).

The observations are plotted in Figures 1–5. The ISI visibility data in Figures 1–4 are plotted first as a function of spatial frequency magnitude (with rising and setting data corresponding to different position angles plotted with different symbols) and then again as a function of position angle (which varies monotonically as the star goes overhead during the course of a night), with each baseline shown separately. Closure phases are shown as a function of the position angle of the shortest baseline, which, given the linear array configuration, was within 1° of all baseline orientations.

For the 2004 September 15–17 ISI data and 2004 September 1 Keck data taken within the same epoch, visibilities agree to within about 5% on baselines that overlap, and the closure phases agree to within about 3°. It should also be noted that for some measurements a closure phase near 20° was obtained, which implies a lower limit to the degree of asymmetry present in the star, which is discussed further in §§ 4–6. For present measurements the visibilities for all three baselines were greater than ~0.3, so the precision of phase closure measurement was good and the asymmetry significant. By contrast, if any visibility in a triangle of three baselines is close enough to zero, even an infinitesimal asymmetry could produce significant nonzero closure phase.

2.2. *Keck Observations*

High-resolution Fourier imaging data were extracted from the Keck telescope using the mid-infrared Long Wavelength Spectrometer (LWS; Campbell & Jones 2004). Following mixed successes in obtaining information up to the full diffraction limit from conventional imaging with this instrument (van der Tak et al. 2005), a novel sparse-aperture interferometric experiment was implemented.

The 36 separate segments that make up the primary mirror of the Keck telescope were individually repointed and rephased using custom software. This enabled the segments to be divided into five subsets. Four of these subsets, consisting of six segments each, formed separate sparse, nonredundant subarrays, with each subarray element being a single 1.8 m hexagonal segment. These interferometric subarrays each gave 15 baselines, ranging between 2.6 and 9.3 m, together with 20 closure phases (10 independent). The phasing and pointing solution for the primary mirror could be arranged so that interference patterns from all four such subarrays could be simultaneously recorded on the LWS detector, so that 24 of the 36 Keck segments were used (the remaining 12 were pointed off-chip).

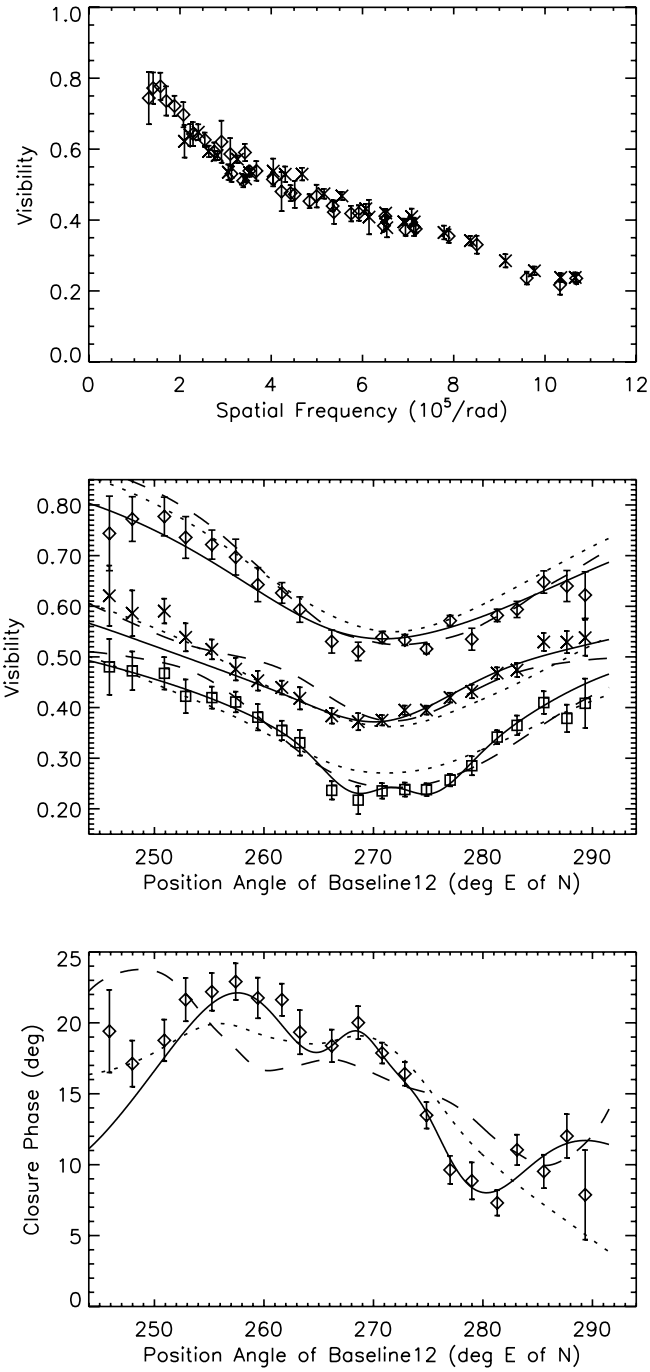

Fig. 1.—ISI visibility and closure phase data from 2004 November 18–19 and various fits. *Top*: Visibility as a function of spatial frequency magnitude. Diamonds refer to data taken as the star was setting, and crosses as it was rising (at different position angles). *Middle*: Same visibility data taken on baselines (1-2; *diamonds*), (2-3; *crosses*), and (3-1; *squares*) as a function of the position angle of baseline (1-2). The maximum spatial frequency corresponds to a position angle of 272°. *Bottom*: Closure phase around the triangle (1-2-3) as a function of position angle of baseline (1-2). The solid line shows the visibility and closure phase for the best-fitting $N = 10$, 12.3% point-source model described in § 5. The dashed line shows the model visibility and closure phase for the image reconstruction technique described in § 6, and the dotted line corresponds to the semiphysical asymmetric dust model considered in § 4.

Data analysis could then proceed in a similar fashion to the long-running Keck aperture-masking experiment implemented in the near-infrared (Tuthill et al. 2000b). Superior calibration of the complex visibilities has been demonstrated by using these sparse-aperture methodologies. Although the conventional wisdom

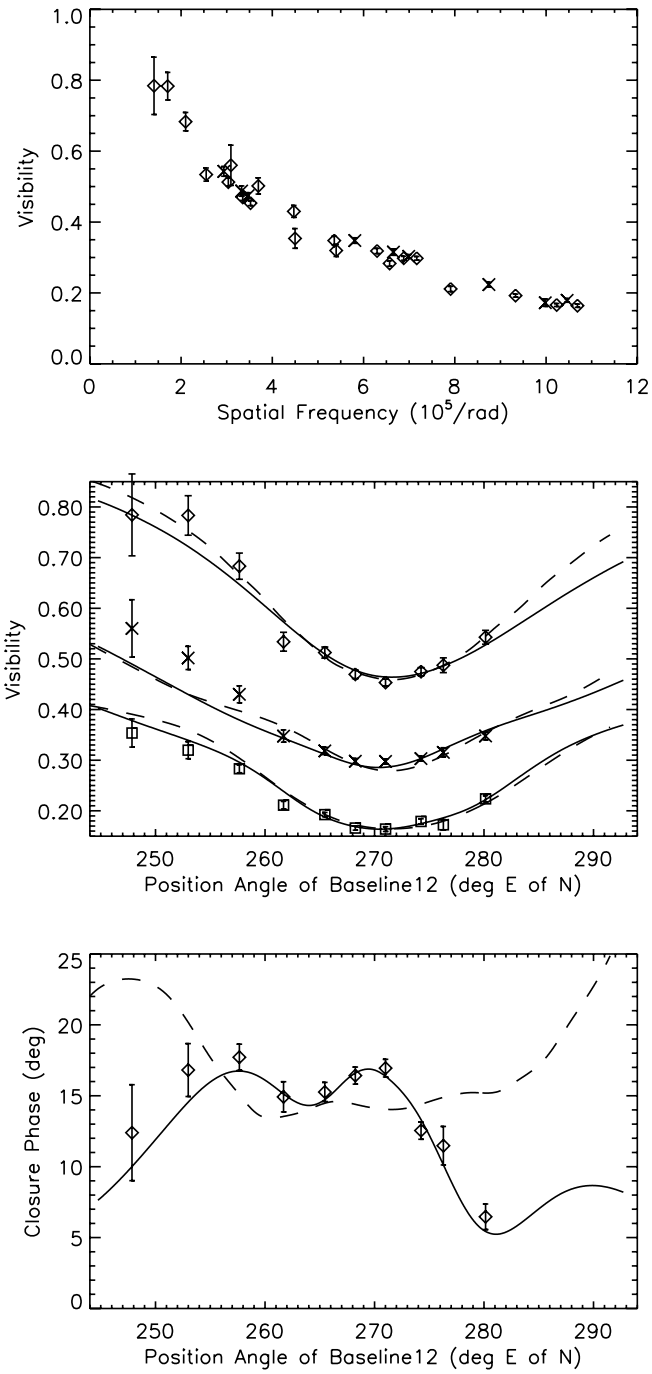

FIG. 2.—Same as Fig. 1, but for data of 2003 December 16–17.

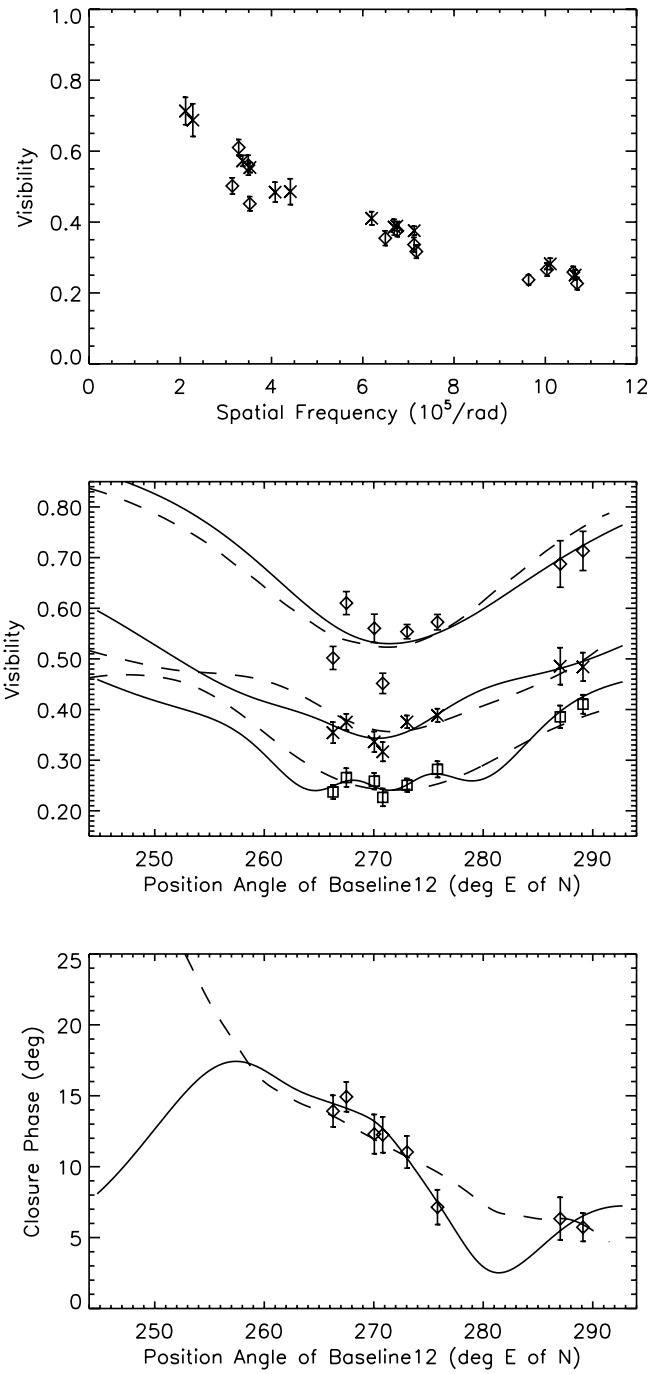

FIG. 3.—Same as Fig. 1, but for data of 2003 September 16–18.

runs that large telescopes can be "nearly diffraction limited" in the mid-infrared, quite to the contrary, we find the regime where the aperture size D is approaching the atmospheric coherence length (r_0) to be one where precise calibration of the complex visibilities is highly challenging (this is sometimes referred to as the "seeing spike" calibration problem). These interferometric methods therefore have great potential to improve mid-IR imaging at large telescopes.

The Keck visibilities are plotted in Figure 5 (*top*) as a function of spatial frequency magnitude. Figure 5 (*middle and bottom*) also contains the Keck closure phases, plotted as a function of the shortest baseline of the three used to construct them, as well as the *u*-*v* coordinates at which the data were obtained. Values of visibility at a given spatial frequency shown in Figure 5 need not necessarily agree because they represent different orientations of baselines having the same length. However, about 5% of the variations in visibility at a given spatial frequency may be due also to imprecision in calibration of visibility measurements for the different baselines.

3. GENERAL COMPARISON WITH PREVIOUS ISI MEASUREMENTS

Observations of IK Tau were made with the ISI during 1992–1995, when it used only two telescopes, and have been previously reported (Danchi et al. 1994; Hale et al. 1997). It was noted then that the visibility curve indicated two dust shell density peaks at distances about 300 and 600 mas from the star and that

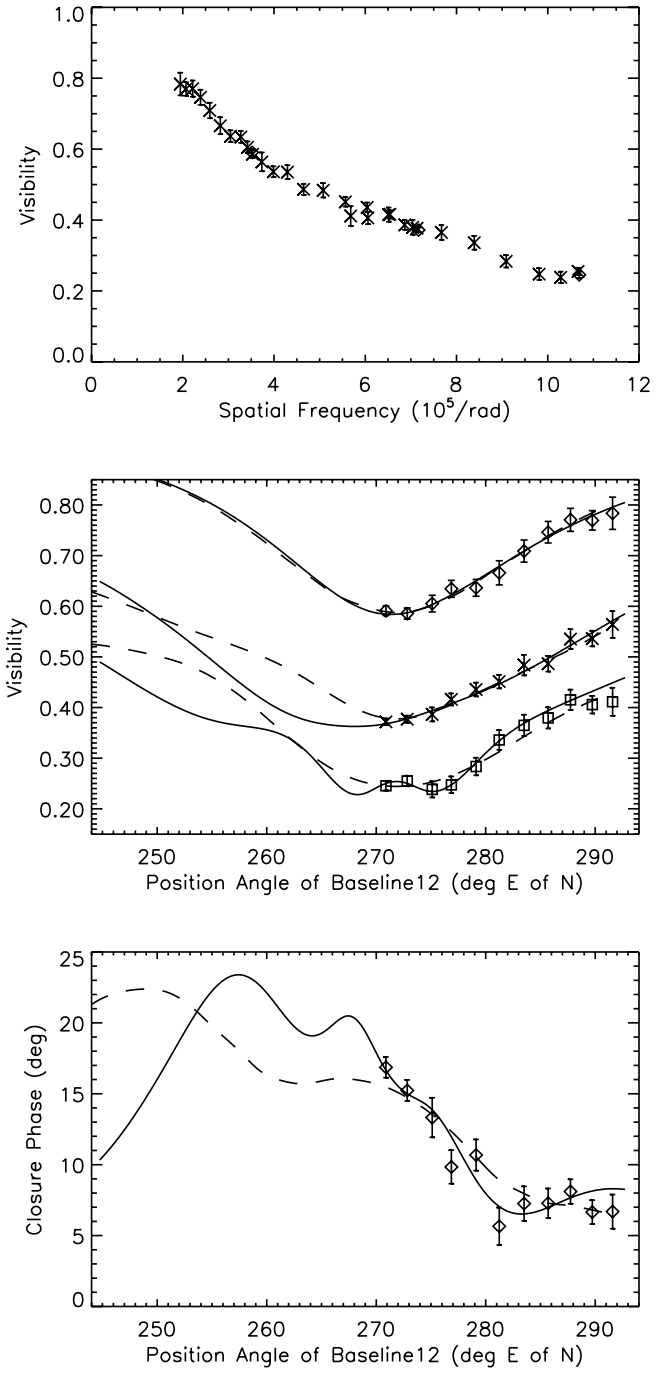

FIG. 4.—Same as Fig. 1, but for data of 2004 September 15–17.

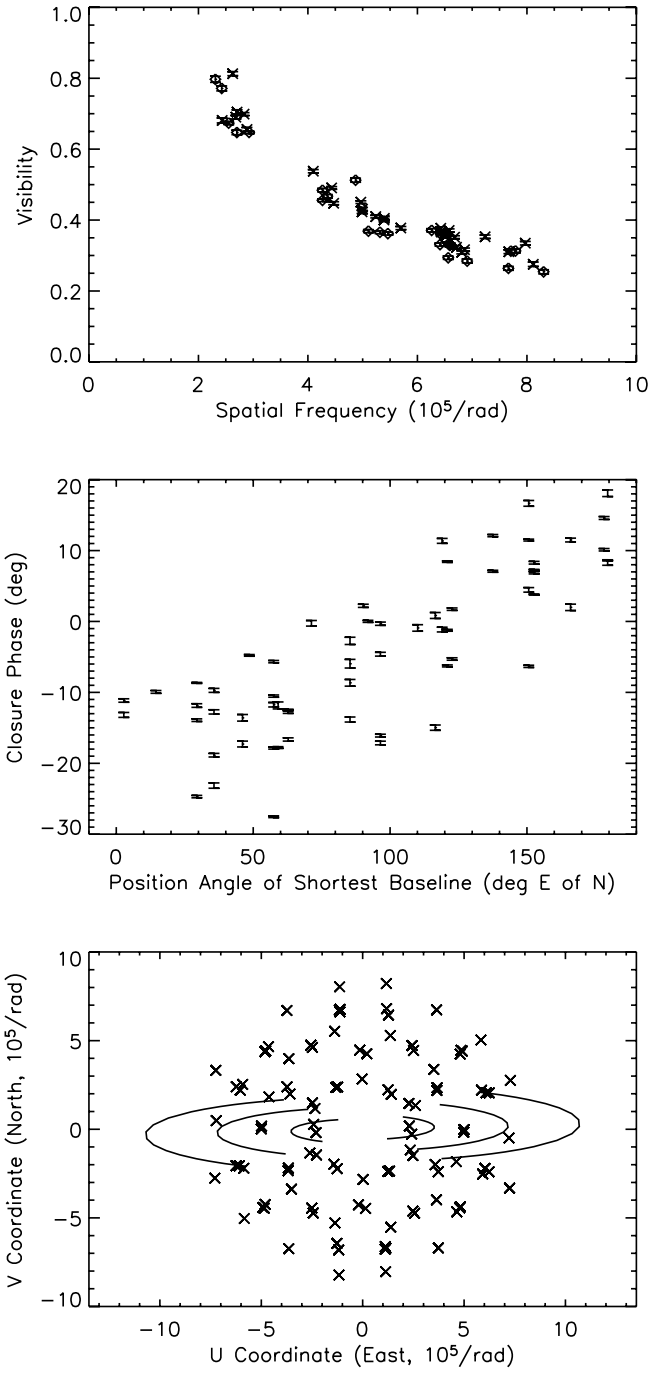

FIG. 5.—Keck single-aperture interferometry visibilities, closure phases, and *u-v* plane. *Top*: Visibility as a function of spatial frequency for points in the northeast (*diamonds*) and northwest (*crosses*) quadrants. *Middle*: Closure phase measurements plotted as a function of the position angle of the shortest leg of the baseline triangle and for many baseline triangles in each case, which produces varied closure phases for a given shortest baseline value. *Bottom*: Points in the *u-v* plane where the Keck data was taken (*crosses*). The ISI coverage of *u-v* values is shown by the overlaid curves.

during 1992–1993 at least the larger shell was moving away from the star at a rate of about 16 mas yr^{-1} (19 km s^{-1}). Hence, a decade later, when the present measurements were made, the shell and probably most of the dust around the star has moved about 160 mas farther away. This would make such a shell somewhat cooler and less luminous, as well as probably more diffuse. Observations in 1992–1993 also show values of visibility much lower than those reported here for 2003–2004 [e.g., approximately half as large at spatial frequencies in the range $(6-8) \times 10^5$ radian^{-1}]. This indicates a substantial decrease over these 10 years in the density of dust surrounding the star.

As previously ejected shells move farther from the central star, the inner regions become more visible at 11 μm. The visibility curve of Figure 1 shows that in the most recent data, a region unresolved by the 12 m baselines of the ISI provides approximately 0.22 of the total flux seen, which is 726 Jy, according to the values in Table 1. Although it is tempting to assign this 726 Jy as radiation directly from the stellar continuum photosphere, this interpretation is not quantitatively consistent with other measurements of IK Tau.

Using the near-maximum photometry of Olivier et al. (2001) at JD 2,447,905, the near-maximum 11 μm photometry of Hale

et al. (1997), *IRAS* fluxes at longer wavelengths, and the American Association of Variable Star Observers (AAVSO) estimate for visual maximum, we can estimate the total received flux from IK Tau at maximum to be 6.2×10^{-9} W m^{-2}. At the distance of 265 pc found by Hale et al. (1997), this gives a bolometric luminosity of 13,400 $L_{\odot}$ at maximum, consistent with the maximum-light period-luminosity relationship of Kanbur et al. (1997) for O-rich Mira variables. Approximating the central star as a 3000 K blackbody, this means that it should have an angular diameter of 15.1 mas and an 11 μm flux density of 230 Jy. The 726 Jy flux unresolved by the recent ISI epochs must therefore come mainly from some combination of newly formed dust and emission from many weak molecular lines in a molecular shell (e.g., see the simple models of Weiner [2004] for o Cet).

The change in 11 μm flux from IK Tau over the last decade is consistent with the observed change in visibility. In 1992–1995, the 11 μm flux at stellar maximum was approximately 5800 Jy (Hale et al. 1997). Table 1 shows a flux of 4600 Jy at stellar maximum in 2003. If the dust were transparent and unchanged in distribution, this would not correspond to a change in visibility of a factor of 2 or more, as observed at relatively high resolutions. However, the dust in 1992 was estimated to have an optical depth of 1.7 at 11 μm (Danchi et al. 1994), which decreased the stellar intensity by a factor of 5.5. The innermost dust, moving at the same rate as that found for more distant shells, would have decreased in density by a factor of 18, decreasing the opacity of 1.7 to about 0.1. Although the opacity of 1.7 could only have been an approximation, as is also this estimate of its change, this shows how the star and associated inner regions can in 2003–2004 be much more apparent at 11 μm than they were in 1992–1995. It also indicates that the emission of material by the star must have very much diminished. Because present measurements show that the dust shell is not a smooth and simple sphere, precise calculations of the changes to be expected in visibility and total flux are not practical, but it is clear that the changes observed in flux are reasonably consistent with observed changes in visibility and indicate a substantially decreased amount of gas or dust emission from IK Tau over the last decade.

Present measurements still show a bump in the visibility curve (see Fig. 1) somewhat similar to the two bumps found in the early 1990s (Danchi et al. 1994). This would indicate some shell-like concentration of dust if spherical symmetry is assumed. Now, however, with the phase closure measurements obtained with three telescopes, symmetry does not need to be assumed, and dust distribution around the star can be more completely determined than it could be in the earlier publication. And because of the large changes in visibility curves and the observed motions, there is also no reason to expect that the present dust distribution and its asymmetries closely resemble that found 10 years earlier. The changes themselves are striking and important.

4. A SEMIPHYSICAL ASYMMETRIC DUST MODEL

A semiphysical asymmetric dust model was designed to provide the simplest and most direct comparison with traditional spherically symmetric dust shells. The model consists of an unresolved stellar component (treated here as a point source of total flux, $F_{\rm star}$) surrounded by a dust shell forming at radius $R_{\rm dust}$ and temperature[1] $T_{\rm dust}$ and having an opacity $\kappa(r, \theta) = \kappa_0 (r/R_{\rm dust})^{-2} (1 + \cos\theta)^{\alpha}$, where θ is the angle between a point on the dust shell and some principal axis of asymmetry, which may be tilted relative to the observer's line of sight and also rotated about it. Furthermore, the dust is assumed to be in LTE at a temperature $T(r) = T_{\rm dust}(r/R_{\rm dust})^{-1/2}$ and the total flux at 11 μm constrained to be 3300 Jy to match ISI flux measurements.

[1] $T_{\rm dust}$ was constrained to be less than 1400 K to match the expected formation of real dust grains.

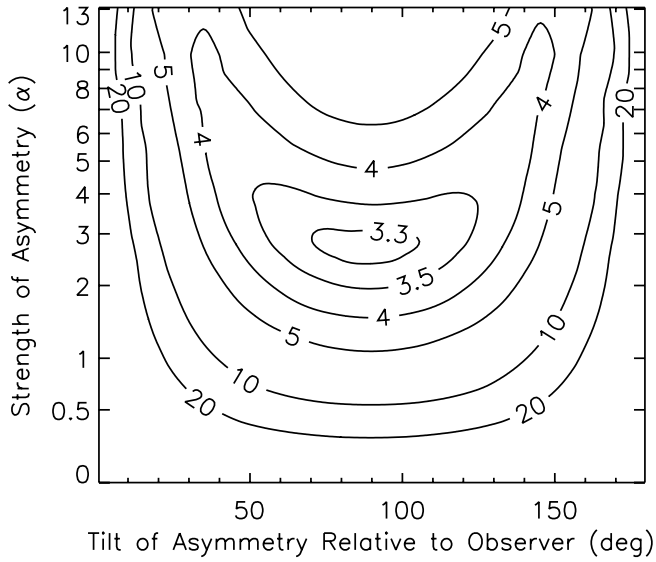

FIG. 6.—χ^2 per data point for the semiphysical asymmetric dust model considered in § 4 fit to the 2004 November 18–19 data set.

Figure 6 shows the χ^2 per data point for this model, using the 2004 November 18–19 ISI data set, as a function of the tilt of the axis of asymmetry relative to the observer and the strength of the asymmetry, α. Minimization with respect to the five other parameters is done for each value of α. Figure 6 indicates that a very strong asymmetry, $\alpha > 2$, is necessary to even coarsely fit the observations. The dotted line in Figure 1 shows the model's fit to the data. The image resulting from the model is in Figure 7. Here north indicates increasing declination, and west indicates decreasing right ascension.

Although this model reproduces the general form of the closure phase and visibility data, it requires an exceptionally large asymmetry in the dust formation (92% of the total dust forms in one hemisphere). Since the radial distribution of dust in this type of model is well constrained, it does not allow for more complex or "clumpier" types of asymmetries, in which dust at larger radii may be the dominant source of the nonzero closure phase, or for possible nonuniform radiation, such as stellar hot spots. The disagreement of this model's parameters with those computed in § 3 indicates that other models should be explored to more realistically fit the data.

5. MINIMUM REQUIRED ADDITIVE ASYMMETRY AND USE OF LOCALIZED INTENSITY VARIATIONS

Since the model of § 4 suggested that the required asymmetry in the dust shell was large, it is clearly important to investigate this directly by trying to fit the data using smaller but more general asymmetries. In this section, the data are fitted to a circularly symmetric image component contributing most of the flux, plus several small point sources, each of equal intensity, constrained to lie within the beam of the ISI. The beam is about 1.″4 in diameter between half-power points. In the limit that the number of point sources becomes large, they can approximate *any* intensity distribution to be added to the circularly symmetric component.

Figure 8 plots the minimum χ^2 per data point for the 2004 November 18–19 data obtainable using N point sources of equal

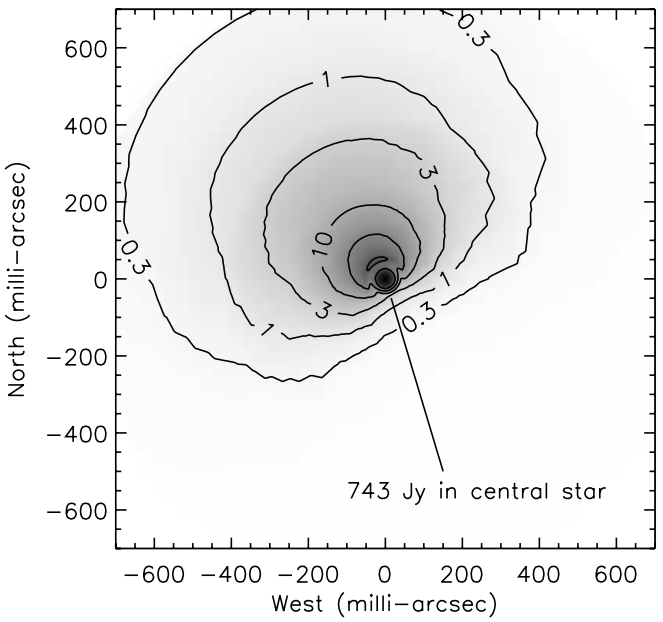

FIG. 7.—Reconstructed image corresponding to the best-fitting semiphysical asymmetric dust model considered in § 4. Contours are in units of mJy mas^{-2} and have values {0.3, 1, 3, 10, 30}. North and west indicate directions of increasing declination and decreasing right ascension, respectively.

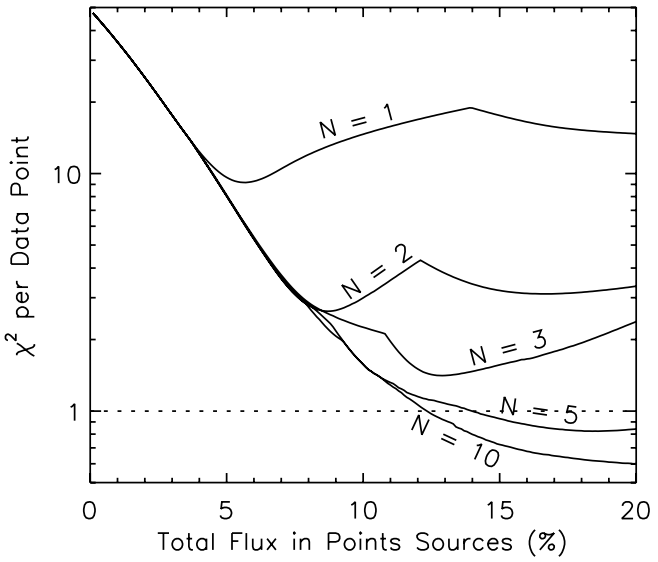

FIG. 8.—Minimum χ^2 per data point for the multiple-point-source model described in § 5 and the 2004 November 18–19 data set. The χ^2 per data point is plotted for the best-fitting cases of 1, 2, 3, 5, and 10 point sources as a function of their total flux.

flux intensity as a function of their total fractional flux[2] for $N = 1$, 2, 3, 5, and 10. The calculations indicate that a lower bound of about 12.3% of the total flux must be contained in the point sources in order to fit the observations. In addition, Figure 8 suggests that even as $N \rightarrow \infty$, there is some minimum fractional flux necessary to fit the observations and that this value is not much below 12.3%.[3] Since stars and their surrounding dust shells are generally approximated as spherical objects, we might consider this *minimum* asymmetry a likely scenario for the cause of the nonzero closure phases. Figures 9 and 10 show the optimized distributions of intensity and point sources, with 12.8% of the total power in the point sources.

Although this technique is one way of formulating a minimum required asymmetry, it is by no means unique. A more likely model is for the point sources to be somewhat enlarged and spread out, although each is still smaller than the spatial resolution, so that a continuous variation in luminosity rather than point sources is obtained. The point sources only show approximately where additional intensity most likely occurs. Similar fits to the phase closure and visibility can also be made by using point sources that decrease in intensity rather than with the increases used in the model illustrated. Each point source of decreased intensity would simply correspond to those shown in Figures 9 and 10, but rotated in position 180° from them. In addition, minor increases in intensity of the circular symmetry pattern with which they are associated would be needed to provide the correct flux and visibilities. This simply shows that, while the present model realistically represents the measured phase closure and asymmetry, it is only a representation rather than being unique.

Figures 9 and 10 show the positions of the required point sources as N progresses from 1 to 10, where the total flux in the point sources is fixed at 12.3% of the total. The circularly symmetry component is also imaged. Although the locations of the points change, a pattern is clearly present. An extra intensity, presumably due to dust density, to the northeast is required to match observations. It also appears that the extra intensity to the north is at larger radii than that to the east. For the $N = 10$ case, the fit to 2004 November 18–19 visibilities and closure phases is shown in Figure 1 to be reasonably good. Radial intensity distributions due to the symmetric dust shell are shown for the different models in Figure 11.

The 2003 December 16–17 data were slightly more limited in coverage than those of 2004 November 18–19, but comparable and at near-maximum luminosity ($\Phi = 0.02$), while the November data were closer to minimum ($\Phi = 0.75$). A model's fit to the somewhat smaller phase closure of 2003 December 16–17 and its visibility are shown in Figure 2, with the model illustrated in Figure 12. The model shows a very similar (although not identical) set of point sources and a larger radius for dust radiation, as can be seen from Figure 11. This smaller radius is to be expected because the dust would be cooler near minimum. Asymmetry in flux due to the 10 point sources is in this case 10.1%, very close to the value that fits the 2004 November 18–19 data. The difference in radial variation of intensity due to the difference in shape of the visibility curves shown by Figures 10 and 13 is somewhat surprising and is presumably due to dust motion, emission, and heating change during the year between the two measurements. According to the estimate given above, the dust is not expected to have moved more than about 16 mas. The change in radial distribution is a bit surprising, but some of this apparent change in radial intensity is probably real, because it seems unlikely that experimental errors alone could produce all of this difference in radial intensity distribution of the models.

Data obtained 2003 September 16–18 and 2004 September 15–17 each contain about half as much u-v plane coverage as that of 2004 November 18–19. Partly as a result of this, the 10-point fit for each set of data can be made with smaller fractional flux asymmetries, namely, 4.3% for 2003 September 16–18 and 4.6% for 2004 September 15–17. The visibility and phase closure fits for

[2] For $N \leq 5$, a unique minimum can be found for the position of each of the point sources. For larger N, good fitting points can be found, but it is too difficult computationally to determine whether they represent an absolute (and unique) minimum.

[3] It can be shown mathematically that without any assumptions of compactness or smoothness, an additive asymmetry must contribute at least 7% to the total flux to create closure phases and visibilities as high as those observed.

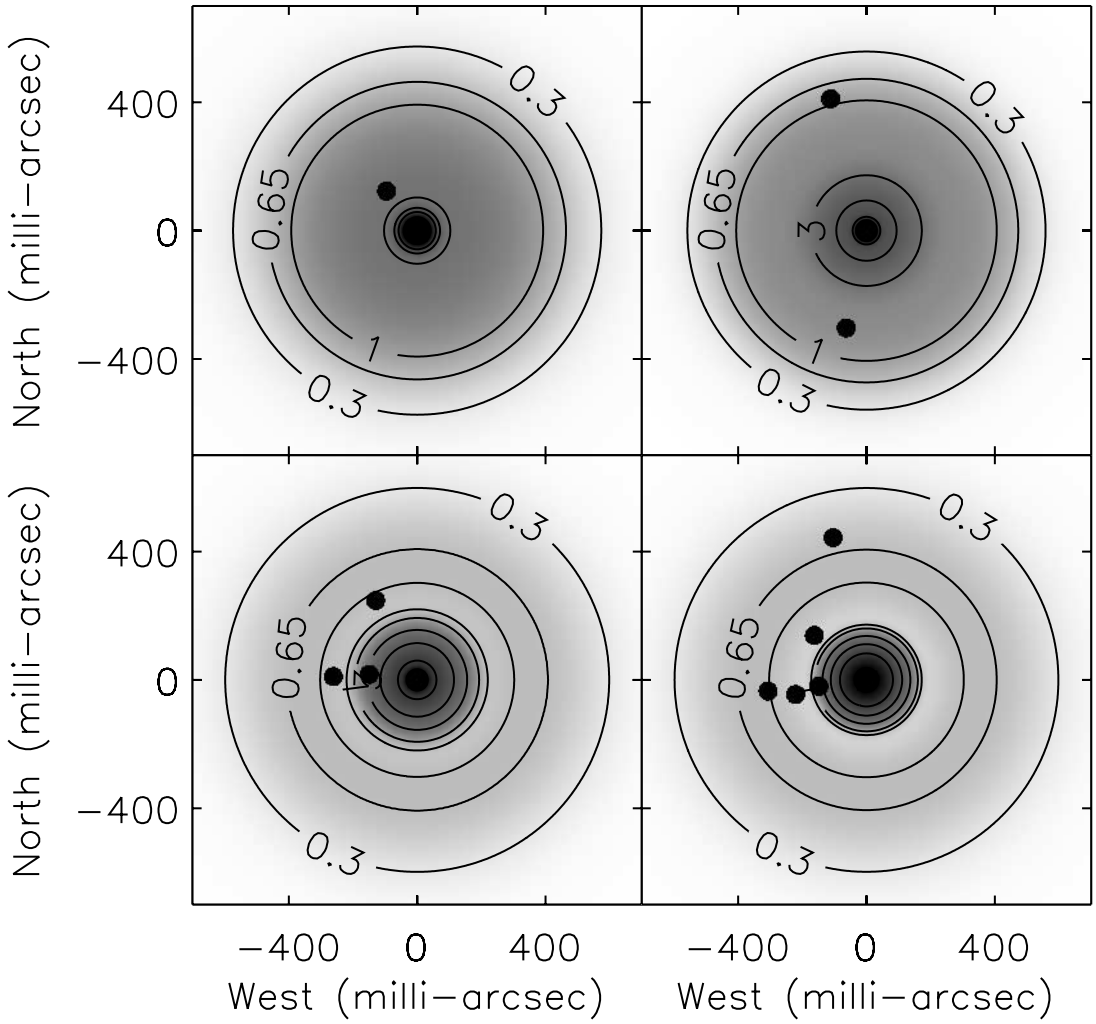

FIG. 9.—Reconstructed images corresponding to the best-fitting 1, 2, 3, and 5 point-source models having a total flux of 12.3% (plus a circularly symmetric component contributing 87.7% of the flux) for the 2004 November 18–19 data. Contours are in units of mJy mas^{-2} and have values {0.3, 0.65, 3, 10, 30}.

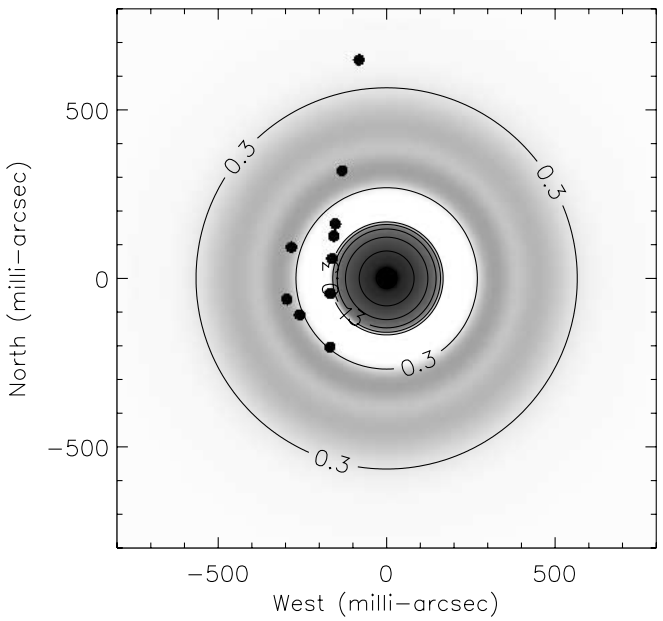

FIG. 10.—Reconstructed image corresponding to the best-fitting 10 point-source model having a total flux of 405 Jy (12.3% of total in the points, plus a circularly symmetric component contributing 87.7% of the flux) for the 2004 November 18–19 data. Contours are in units of mJy mas^{-2} and have values {0.3, 1, 3, 10, 30}.

these two cases are shown in Figures 3 and 4. Again, the point sources representing asymmetry are very similar in position to those found for other dates, although they are weaker in intensity. All four models show greater intensity toward the north and a general extension of intensity toward the east. Images of the models are in Figures 13 and 14. Figure 14, representing the radial distribution and point-source asymmetry for 2004 September 15–17, shows a more concentrated radial distribution that any of the others. This is to be expected because it represents data very near the minimum luminosity of the star ($\Phi = 0.61$). The Keck results are discussed in detail in § 7.

6. GENERALIZED IMAGE RECONSTRUCTION

A completely general modeling approach would be to devise an infinite or large number of continuous orthogonal functions whose amplitudes could then be constrained by the data. But to avoid the difficulty inherent in this approach, we use only a small number of continuous functions, enough to allow substantial flexibility for the basic structure of the model, but not with so many that analysis becomes cumbersome.

The object is assumed to consist of a point source, which is the star, plus a bloblike intensity distribution representing the surrounding material, with an angular size no larger than the beam of a single telescope. Although the blob can have some structure, it is smooth enough that, except for the star, none is small enough

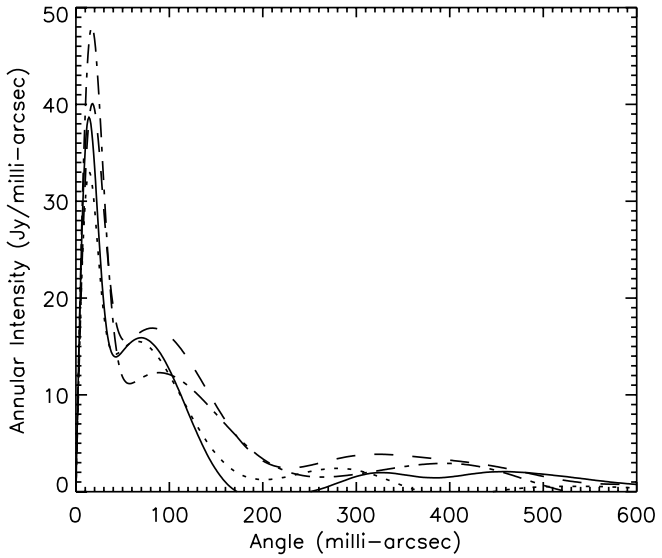

FIG. 11.—Annular Intensity in the circularly symmetric component of the multiple-point-source image reconstruction described in § 5. The intensities for 2004 November 8–19, 2004 September 15–17, 2003 December 16–17, and 2003 September 16–18 are given by the solid, dotted, dashed, and dashed-dotted curves, respectively.

to affect the highest resolutions provided by present measurements. The flux intensity I_* is modeled to have the form

$$I_* = e_0\delta(r) + (a + b + c + d)\exp\left[\frac{-r^2}{(1+\alpha+\beta)\sigma^2}\right],$$

where

$$a = a_0, \quad b = b_0\left(r - \tfrac{1}{4}\right),$$
$$c = c_0(24r^2 - 12r + 1),$$
$$d = d_0(160r^3 - 120r^2 + 24r - 1),$$
$$\alpha = \alpha_0\cos(\theta + \phi_1), \quad \beta = \beta_0\cos(2\theta + \phi_2).$$

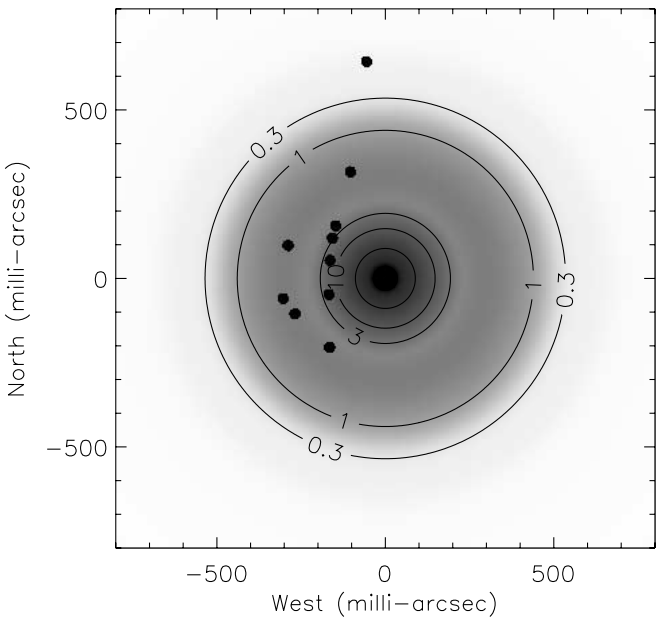

FIG. 12.—Same as Fig. 10, but for 2003 December 16–17 data and with point sources having a total flux of 405 Jy (8.8% of total). Contours are in units of mJy mas^{-2} and have values {0.3, 1, 3, 10, 30, 100}.

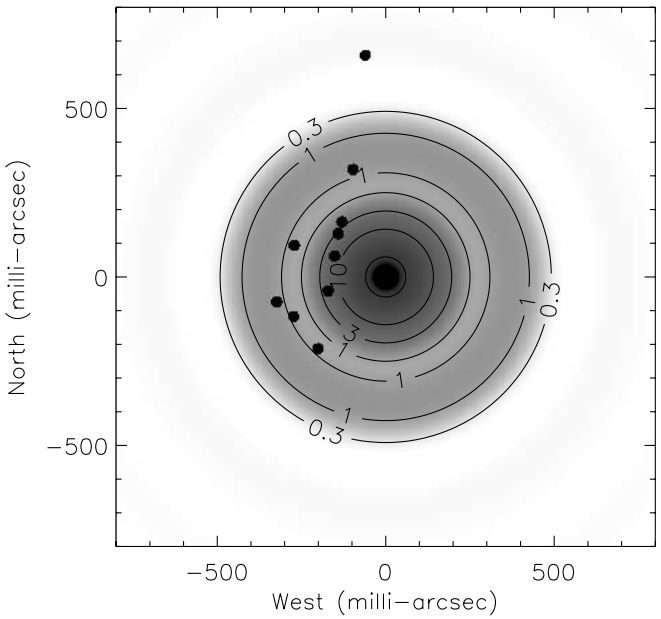

FIG. 13.—Same as Fig. 10, but for 2003 September 16–18 data and with point sources having a total flux of 405 Jy (10.4% of total). Contours are in units of mJy mas^{-2} and have values {0.3, 1, 3, 10, 30, 100}.

The coefficients a_0, b_0, c_0, and d_0 are the amplitudes of the polynomial functions, radially modifying the otherwise Gaussian function of the radius. Furthermore, α_0, β_0, ϕ_1, and ϕ_2 are the amplitudes and phases of the functions that vary the width of the Gaussian with angle. Finally, e_0 is the strength of the point-source star represented by a delta function at the position $r = 0$. The polynomials, which are orthogonal over the range $[0, \frac{1}{2}]$, are designed to vary the form of the blob at different distances from the center, and the α- and β-terms produce dipole and quadrupole moments in the image. Individually, they yield a lopsided image and an elongated image, respectively. The angles ϕ_1, and ϕ_2 determine the directions of the asymmetry and elongation, respectively.

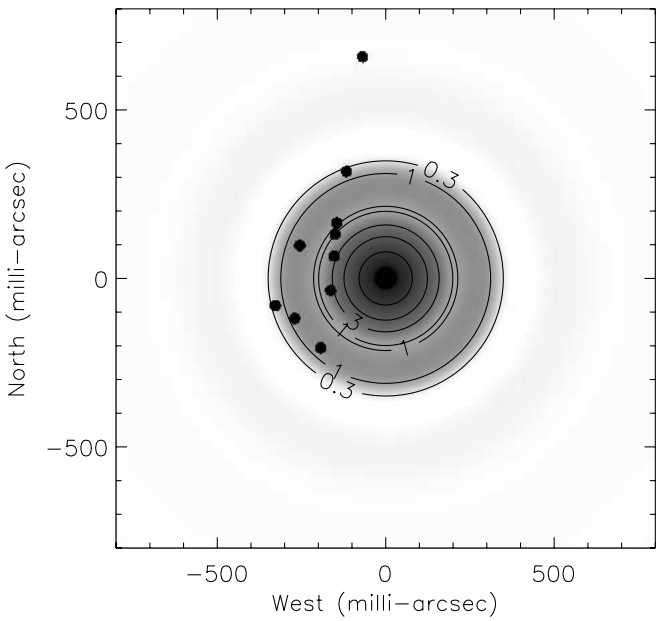

FIG. 14.—Same as Fig. 10, but for 2004 September 15–17 data and with point sources having a total flux of 405 Jy (13.5% of total). Contours are in units of mJy mas^{-2} and have values {0.3, 1, 3, 10, 30, 100}.

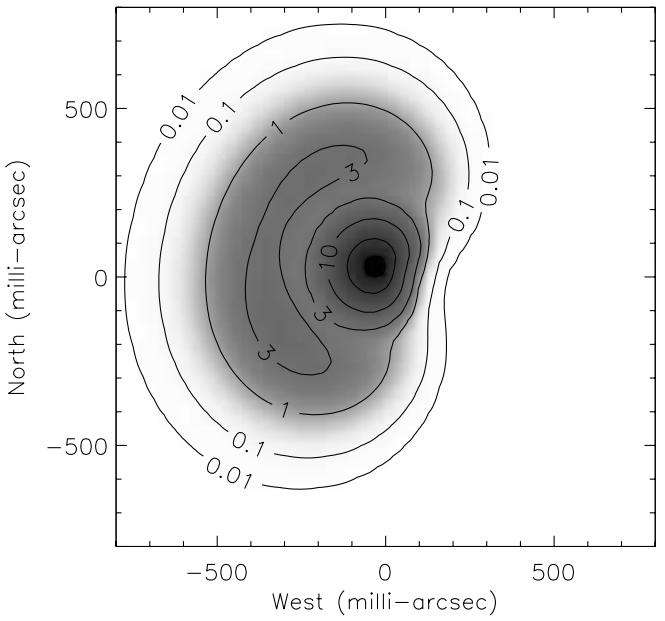

FIG. 15.—Generalized image reconstruction (described in § 6) for the 2004 November 18–19 data set. Contours are in units of mJy mas^{-2} and have values {0.01, 0.1, 1, 3, 10, 30, 100}.

The polynomials were iteratively fit to the data starting with a featureless Gaussian of reasonable width, while α and β were set to zero. With the polynomial coefficients fixed, α and β were then adjusted for a best fit, after which all parameters were allowed to change to provide the most perfect fit. The results are shown as a possible image in Figure 15 for the most complete data set, taken in 2004 November. How well these types of images fit measured ISI visibility and closure phase data can be seen in Figures 1–4. Images of other dates are not shown, as the model is particularly sensitive to the parts of the *u-v* plane that are sampled and optimally fitted, and sensitive to small variations or errors in the data to be fitted.

The comparatively sparse data of the other sets resulted in unrealistic artifacts in the image. Results in fitting the Keck data are discussed in § 7. Better fits than those obtained may exist, but they were not found, and this is unlikely due to the small number of parameters used. A coarse sampling of all variations of this model was performed by making over 2000 different guesses for initial parameter values, but none converged to better fits than those shown.

Visibility curves are fitted rather well for all data sets with this model, including the Keck data. However, this smooth model failed to adequately fit closure phases of the 2003 December 16–17 or 2004 November 18–19 data. It proved unable to fit the closure phases of the Keck data over the large number of baseline orientations. The model generally converged to an image that fit only the visibilities, but had zero closure phase at all baselines. Attempts to improve the fits included adding higher order polynomials to modify the Gaussian, but optimization of these gave them near-zero coefficients because the visibility was already well fit. Adding sinusoidal variations of higher frequencies to alter the azimuthal structure did not succeed in improving the fits significantly either. However, the use of many localized point sources did fit these data, as shown in § 5. This suggests that, although the closure phase does not directly indicate how each of the three spatial frequencies contributes to the closure phase, we may conclude that a significant portion of the asymmetry comes from the more complex and high-frequency features of the image. Asymmetry due to details revealed only at high resolutions is not surprising, since the lower visibilities at higher resolution allows small variations in intensity to generate significant values of phase closure. Some of the failure of this model to fit phase closure may also be due to the limitations in the geometries that the model allows. For example, it does not allow anything like a spiral-shaped structure.

Variations in the fitted images that increased χ^2 by no more than a factor of 2 were explored to determine how strongly different features of the image are constrained. To do this effectively, the parameters were varied in specific combinations that modify only one independent characteristic of the image at a time. The combinations used were derived using principal component analysis to eliminate covariance of the parameters under small changes and determine which the fitting is most sensitive to. Moderate changes in the north-south symmetry, or in the amount of indentation on the westward side of the image, did not have strong effects on the quality of the fit. One of the most strongly constrained characteristics is the intensity ratio of the star to the dust shell, since that alters the results over a wide range of resolutions. With the exception of the 2003 December 16–17 data, the ratio of stellar to total intensity was quite close to 16%. For the 2003 December 16–17 data, it was approximately 11%, presumably because the star's greater luminosity increased the dust luminosity.

7. THE KECK TELESCOPE AND RESULTS

The wealth of visibility and closure phase data provided by interferometric measurement with the Keck telescope cannot be fitted well using a modest number of small perturbation functions with a mostly circularly symmetric image. However, it can be fitted quite practically and reasonably well by using a symmetric radial distribution of intensity as a major dust shell contribution, a central unresolved star, and a number of point sources approximately placed to provide the asymmetry and phase closure indicated by the measurements. This type of modeling is essentially the same as that used to fit the ISI data in § 5 above. Fifty equal intensity point sources rather than 10 were used because of the more extensive data supplied by the Keck measurements. The resulting model is shown in Figure 17. The residuals are shown in Figure 16. Errors in visibility measurements shown represent the precision of an individual measurement. However, calibration errors in individual baselines were about 5%, which is why a much more extensive effort to fit the data better than the present model is probably not justified.

Data were taken with the Keck telescope at a stellar phase of 0.58, closer to minimum than any of the ISI observations. This makes the relatively small size of the dust distribution for the resulting model shown in Figure 17 reasonable. It is even somewhat smaller than the model that fits the ISI measurements of 2004 September 15–17, from Keck data close to the same phase and time. The Keck instrument used wavelengths centered at 10.7 μm, while the ISI operated at 11.15 μm, and at the shorter wavelengths the flux produced by low-temperature dust would be smaller, which may contribute to the somewhat smaller size. Asymmetries used for modeling the Keck measurements are more detailed than those used for modeling the more limited ISI data. But the general nature of this asymmetry, with intensity increased to the east and extended toward the north, is quite similar. And the total fraction of asymmetric intensity for this model is 16%, in good agreement with most of the models of ISI data discussed in § 4. It is also in good agreement with the value of 12.3% of asymmetric flux found in the point modeling of asymmetry in § 5 for data of 2004 November 18–19, the most complete set obtained with the ISI instrument.

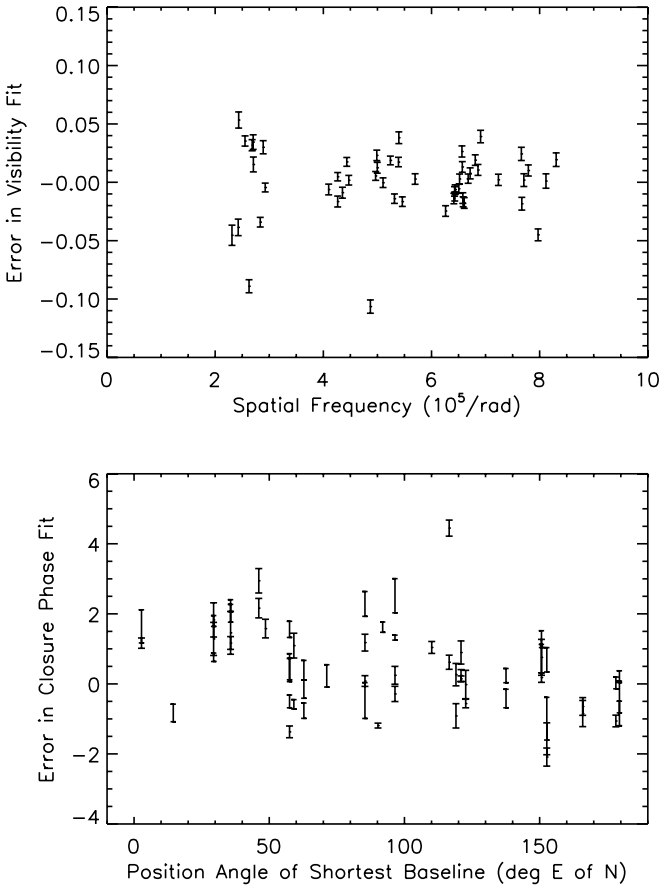

FIG. 16.—Residuals for the visibilities and closure phases for the best-fitting 50 point source, 16% fractional flux model for the Keck single-aperture interferometry data. Error bars represent experimental measurement errors.

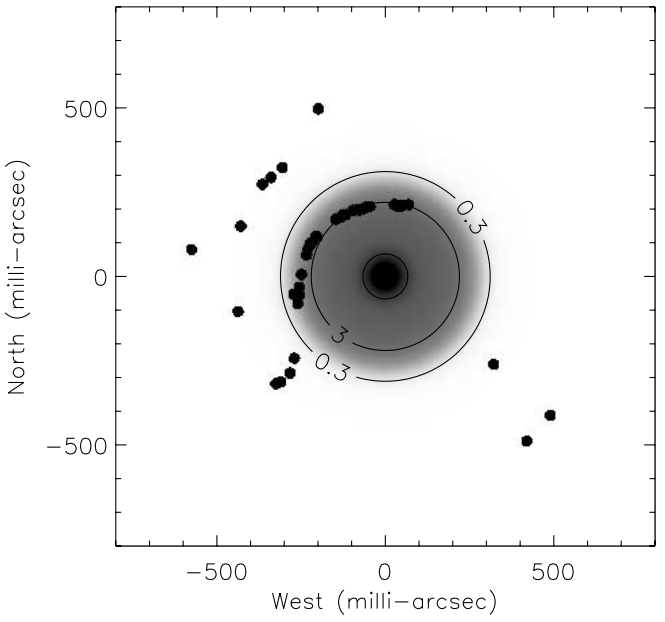

FIG. 17.—Same as Fig. 10, but for the Keck single-aperture interferometry, and using 50 point sources contributing a total flux of 16%. Contours are in units of mJy mas^{-2} and have values {0.3, 3, 30, 100}.

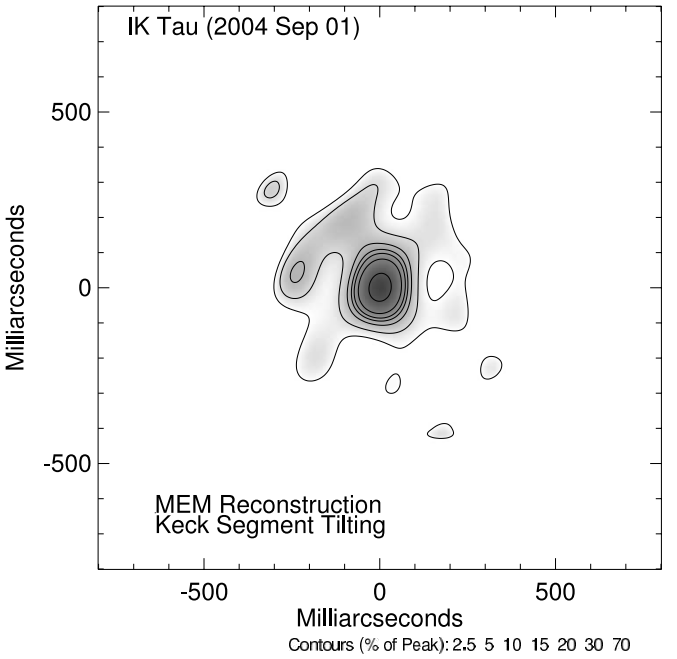

FIG. 18.—Model of intensity distribution for results of the Keck single-aperture interferometry using the maximum entropy method (MEM). This can be compared with Fig. 17.

Attempts to fit the Keck data visibilities using the method described in § 6 were fairly successful, although fitting the closure phase was not possible at all. This is most likely due to the lack of high-frequency asymmetry in the perturbed Gaussian model. The Keck data show a great deal of variation in the measured phases. Since the asymmetries are likely due to high spatial frequencies, this method using a limited number of variables is unable to fit the varied and significant closure phases.

No fit to the Keck interferometry data could be obtained having a χ^2 per data point of unity for small perturbations of a mostly circularly symmetric image. This may be largely due to the fact that probable errors given for the data represent fluctuations in measurements on an individual baseline, whereas the calibration errors of visibility measurements of various baselines were probably rather larger. However, the general form of the visibility and closure phase could be reproduced using 50 point sources contributing 16% of the total flux plus a circularly symmetric object.[4]

The Keck data have also been fitted by using the maximum entropy method (MEM; Cornwell & Evans 1985), which yields a continuum intensity distribution rather than one with point sources. The result is shown in Figure 18. It is clear that the two modeling methods, illustrated in Figures 17 and 18, agree rather well in their general intensity distributions. Overall, the data and models provided by the Keck and ISI instruments agree rather well and probably give a fairly accurate description of the stellar and dust intensity pattern at 11 μm, including asymmetries revealed by phase closure measurements.

8. CONCLUSIONS

Interferometric measurements at 11 μm wavelengths on IK Tau in 2003–2004 compared with those of 1993–1994 show that the dust density surrounding the star has changed considerably, the later observations showing somewhat less shell structure and

[4] The Keck data set spans a larger region of the u-v plane than does the ISI data set and thus required a larger number of point sources to fit it.

more transparency, with dust emission surrounding the star having decreased substantially during the decade. As a result, the visibility at higher spatial frequencies is about 4 times larger in 2003–2004 than during the earlier measurements. If this were solely a change in the stellar contribution, this would indicate an increase in its estimated diameter from the previous estimate of about 18 mas to the range 25–31 mas. However, bolometric luminosity data indicate that the actual stellar contribution may be much less, resulting in an estimate of approximately 15.1 mas.

Inspection of the ISI visibility curves from the four epochs shows a general similarity, but with some clear changes, particularly at higher spatial frequencies. Much of this can be accounted for by changing the stellar contribution of the model to raise the visibilities at higher spatial frequencies. Evidence that some of this extra visibility may come from turbulent structure in the dust shell, or sharp edges to the inner dust regions, may help to account for the small but persistent differences in the visibility curves even after altering the stellar contribution. The final resolution to the question of where the high-frequency structure comes from can be resolved by future measurements. If the structure is predominantly dust in the inner regions of the star that are shadowing outer dust, then in a decade's time the illumination of the outer dust can be expected to change drastically as the inner dust shell evolves. If, however, the change in high-frequency visibility is mainly due to a changing stellar contribution, we may expect the visibility curves in the future to be similar to those observed recently.

Phase closure measurements provided by the recent addition of a third telescope for the ISI instrument, as well as by the use of the many individual segments of the Keck telescope to provide interferometry, show that the dust shell is substantially asymmetric, with perhaps 15% more intensity on one side than on the other. The expected variations in the radii at which appreciable radiation comes from in the dust shell is observed with variations in stellar luminosity.

Such asymmetries are in line with expectations when compared to maps of the masers surrounding IK Tau. The positions of these masers have been measured by other interferometers (Boboltz & Diamond 2005; Bains et al. 2003). The SiO masers mapped by Boboltz & Diamond (2005) are quite close to the star, before the region of dust formation. There is no detailed correlation between the asymmetries of the masers and dust shell, presumably because the dust is located an order of magnitude farther out than the SiO maser region.

Although a complete and precise image of the dust shell cannot easily be made, a number of methods to obtain approximate and practical models of the dust distribution are discussed. Models using data from Keck and from ISI, which are two quite different instruments, agree well. Inspection of Figures 15, 17, and 18, show the same general structure of the surrounding dust. Considering the varied approaches used and that two different data sets are used for the various images, the degree of similarity is striking. All three have an arclike structure about 200 mas to the northeast. This also implies a common lesser intensity to the west side of the image.

This research has been helpfully supported by the Office of Naval Research, the National Research Foundation, NASA, and the George and Betty Moore Foundation. It has made use of the SIMBAD database and the Keck Observatory.

REFERENCES

Bains, I., Cohen, R. J., Louridas, A., Richards, A. M. S., Rosa-Gonzáles, D., & Yates, J. A. 2003, MNRAS, 342, 8
Baldwin, J. E., Haniff, C. A., Mackay, C. D., & Warner, P. J. 1986, Nature, 320, 595
Biller, B. A., et al. 2005, ApJ, 620, 450
Boboltz, D. A., & Diamond, P. J. 2005, ApJ, 625, 978
Campbell, R. D., & Jones, B. 2004, Adv. Space Res., 34(3), 499
Cornwell, T. J., & Evans, K. F. 1985, A&A, 143, 77
Danchi, W. C., Bester, M., Degiacomi, C. G., Greenhill, L. J., & Townes, C. H. 1994, AJ, 107, 1469
Hale, D. D. S., Fitelson, W., Monnier, J. D., Weiner, J., & Townes, C. H. 2003, in Proc. SPIE, 4838, 387
Hale, D. D. S., et al. 1997, ApJ, 490, 407
———. 2000, ApJ, 537, 998
Kanbur, S. M., Hendry, M. A., & Clarke, D. 1997, MNRAS, 289, 428
Monnier, J. D., Tuthill, P. G., & Danchi, W. C. 2000, ApJ, 545, 957
Monnier, J. D., et al. 1997, ApJ, 481, 420
———. 2004, ApJ, 605, 436
Olivier, E. A., Whitelock, P., & Marang, F. 2001, MNRAS, 326, 490
Soker, N., & Zoabi, E. 2002, MNRAS, 329, 204
Suh, K.-W. 2002, MNRAS, 332, 513
Tuthill, P. G., Monnier, J. D., & Danchi, W. C. 1999, Nature, 398, 487
———. 2005, ApJ, 624, 352
Tuthill, P. G., Monnier, J. D., Danchi, W. C., & Lopez, B. 2000a, ApJ, 543, 284
Tuthill, P. G., Monnier, J. D., Danchi, W. C., Wishnow, E. H., & Haniff, C. A. 2000b, PASP, 112, 555
van der Tak, F. F. S., Tuthill, P. G., & Danchi, W. C. 2005, A&A, 431, 993
Vinković, D., Blöcker, T., Hofmann, K.-H., Elitzur, M., & Weigelt, G. 2004, MNRAS, 352, 852
Weiner, J. 2004, ApJ, 611, L37